Supplementary Information for:

Optimum in Ligand Density for Conductivity in Polymer Electrolytes

Nicole S. Schauser,[†,‡,¶] Peter M. Richardson,[‡,¶] Andrei Nikolaev,[§,¶]

Piper Cooke,[‡,§] Gabrielle A. Kliegle,[‡,§], Ethan M. Susca,[‡] Keith Johnson,[†,‡]

Hengbin Wang,[¶] Javier Read de Alaniz,[§] Raphaële Clément, [*,‡,†,¶] and

Rachel A. Segalman[*,‡,†,⁄,¶]

†*Materials Department*
University of California, Santa Barbara, California 93106, United States

‡*Materials Research Laboratory*
University of California, Santa Barbara, California 93106, United States

¶*Mitsubishi Chemical Center for Advanced Materials*
University of California, Santa Barbara, California 93106, United States

§*Department of Chemistry and Biochemistry*
University of California, Santa Barbara, California 93106, United States

‖*Department of Chemical Engineering*
University of California, Santa Barbara, California 93106, United States

Contents

Solution-state NMR:

Grafting densities were determined by integration of NMR data. For the ethane-imidazole series, the imidazole peaks (located between 6.8 and 7.7 ppm) were compared with the integration of the methyl group on the siloxane backbone (located around 0.1 ppm):

$$\%\ imidazole\ grafting, PVMS-Et-Im = \frac{Imidazole\ C_2\ proton}{Backbone\ methyl\ protons/3} \times 100 = \frac{300}{Backbone\ methyl\ protons}$$

For the phenyl-imidazole series, the ratio of the phenyl aromatic protons to imidazole aromatic protons was used. The phenyl protons overlap with one (or two, in the case of the 14% grafted) imidazole protons, and thus the following equations were used:

$$\%\ imidazole\ grafting, PVMS-Phc-Im = \frac{Imidazole\ C_2\ proton}{(Middle\ aromatic\ protons-1)/5} \times 100 = \frac{500}{(Middle\ aromatic\ protons-1)}$$

and for the 14%:

$$\%\ imidazole\ grafting, PVMS-Phc-Im\ 14 = \frac{Imidazole\ C_2\ proton}{(Middle\ aromatic\ protons-2)/5} \times 100 = \frac{500}{B(Middle\ aromatic\ pro}$$

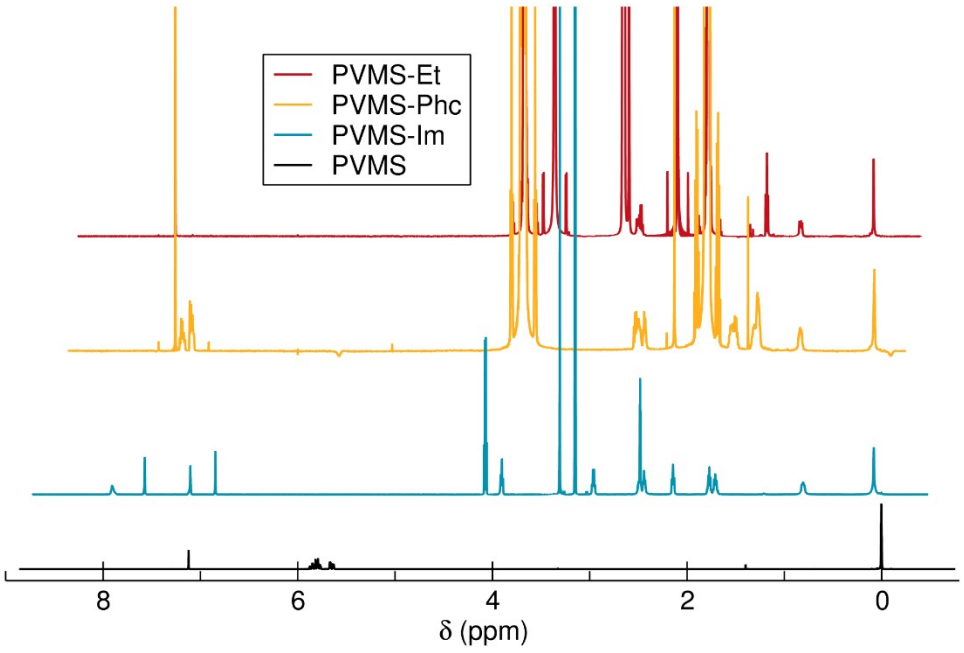

Figure S1. NMR traces of PVMS before and after functionalization with ethane-thiol, phenyl-thiol or imidazole-thiol. The disappearance of the allyl peaks between 5.5 and 6 ppm suggests full conversion.

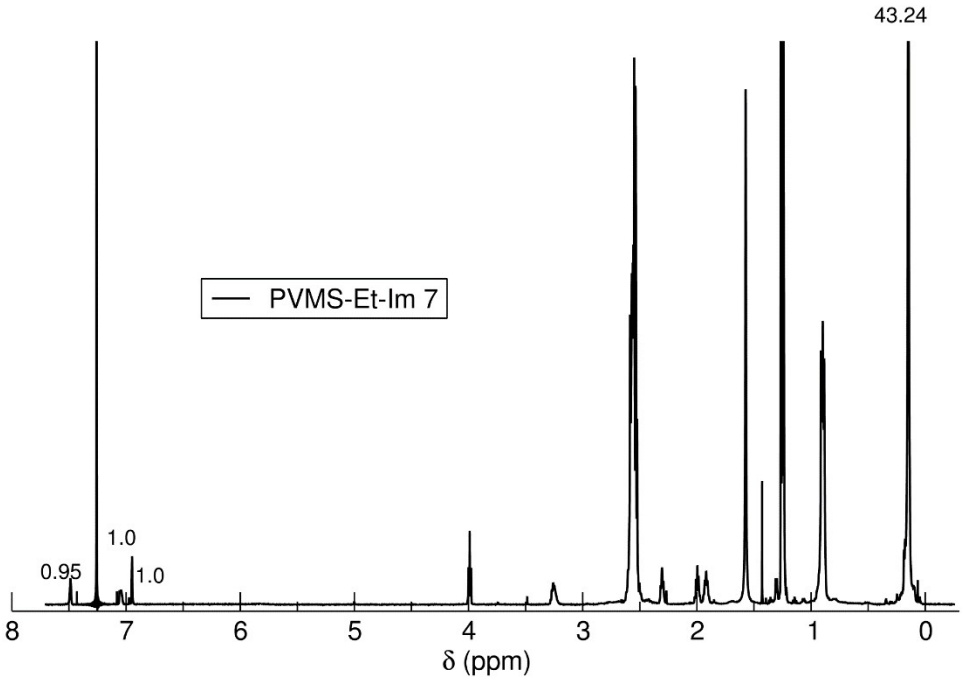

Figure S2. NMR trace for PVMS-Et-Im with 7% imidazole grafting showing integration ratio between the imidazole aromatic peaks and the siloxane backbone. Taken in $CDCl_3$.

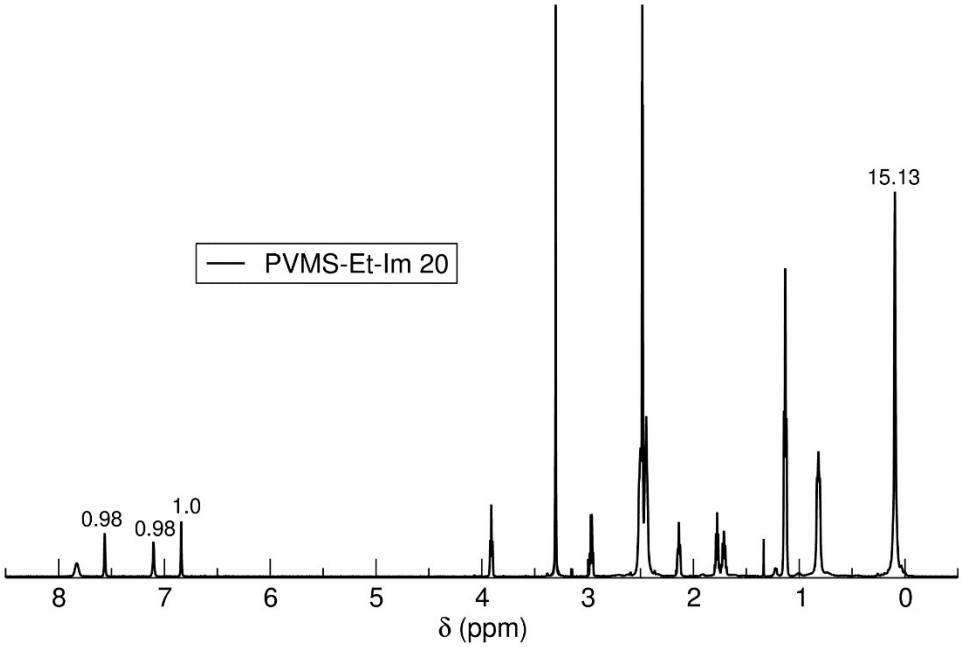

Figure S3. NMR trace for PVMS-Et-Im with 20% imidazole grafting showing integration ratio between the imidazole aromatic peaks and the siloxane backbone. Taken in DMSO-d6.

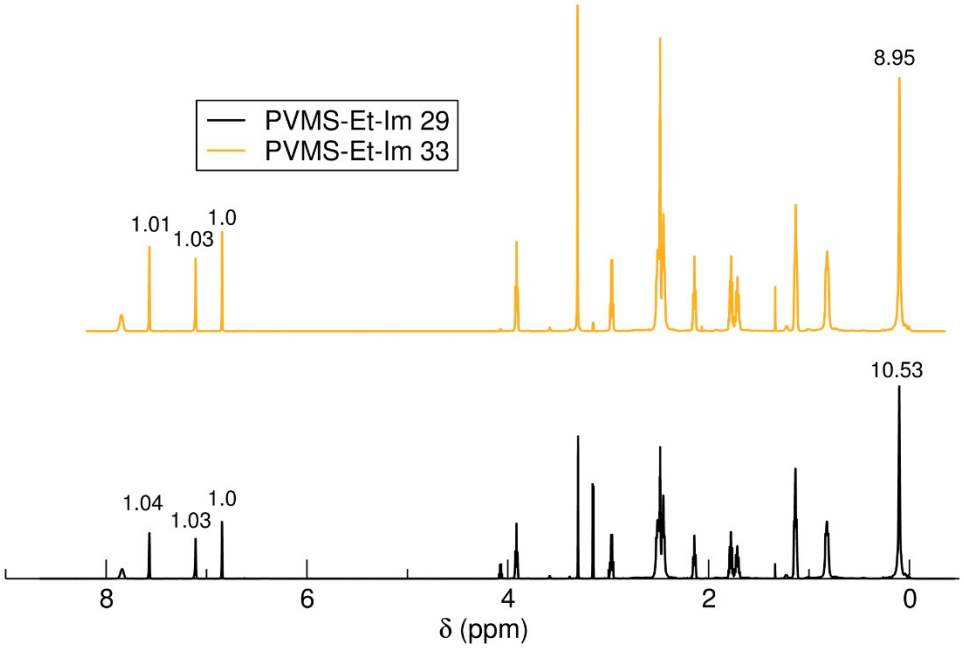

Figure S4. NMR trace for PVMS-Et-Im with 29% (bottom) and 33% (top) imidazole grafting showing integration ratio between the imidazole aromatic peaks and the siloxane backbone. Taken in DMSO-d6.

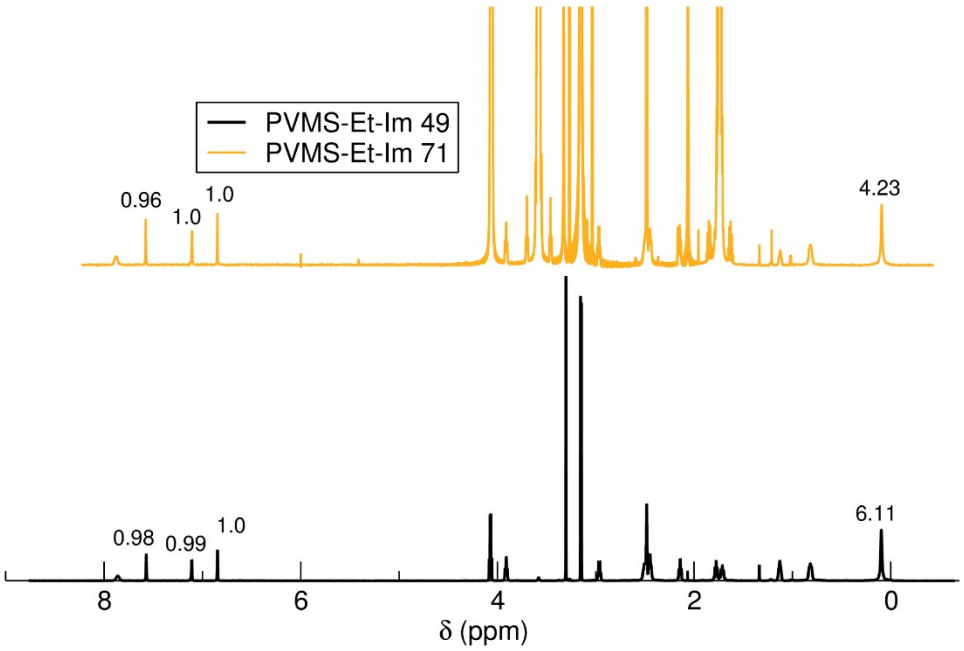

Figure S5. NMR trace for PVMS-Et-Im with 49% (bottom) and 71% (top) imidazole grafting showing integration ratio between the imidazole aromatic peaks and the siloxane backbone. Taken in DMSO-d6.

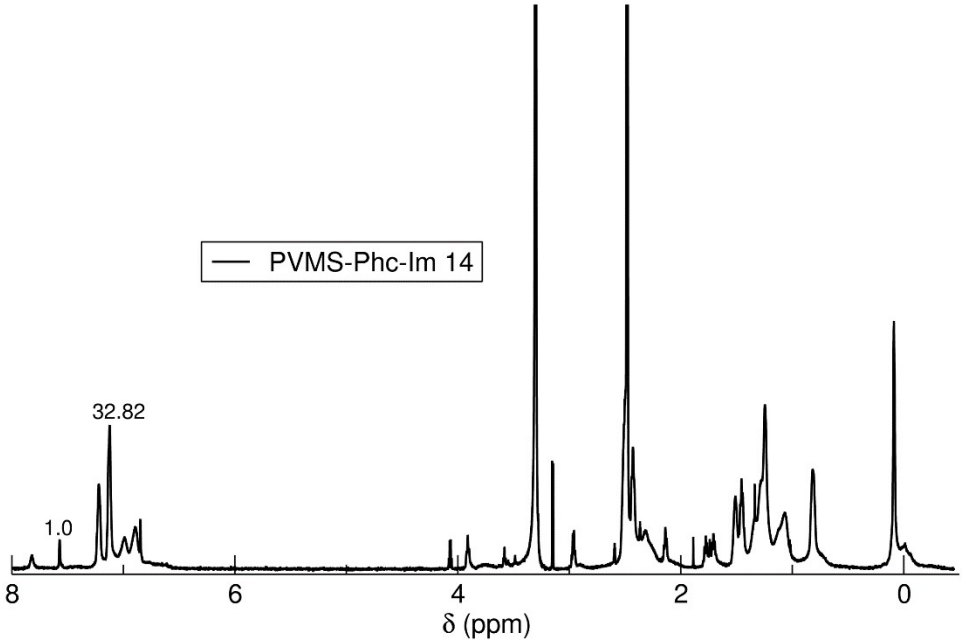

Figure S6. NMR trace for PVMS-Phc-Im with 14% imidazole grafting showing integration ratio between the imidazole and phenyl aromatic peaks. Taken in DMSO-d6.

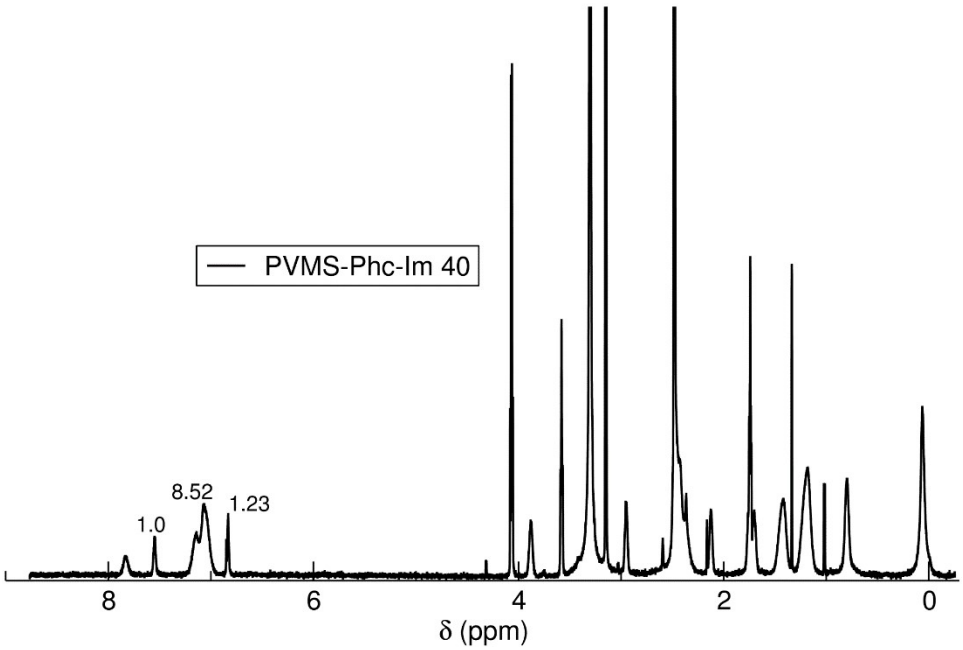

Figure S7. NMR trace for PVMS-Phc-Im with 40% imidazole grafting showing integration ratio between the imidazole and phenyl aromatic peaks. Taken in DMSO-d6.

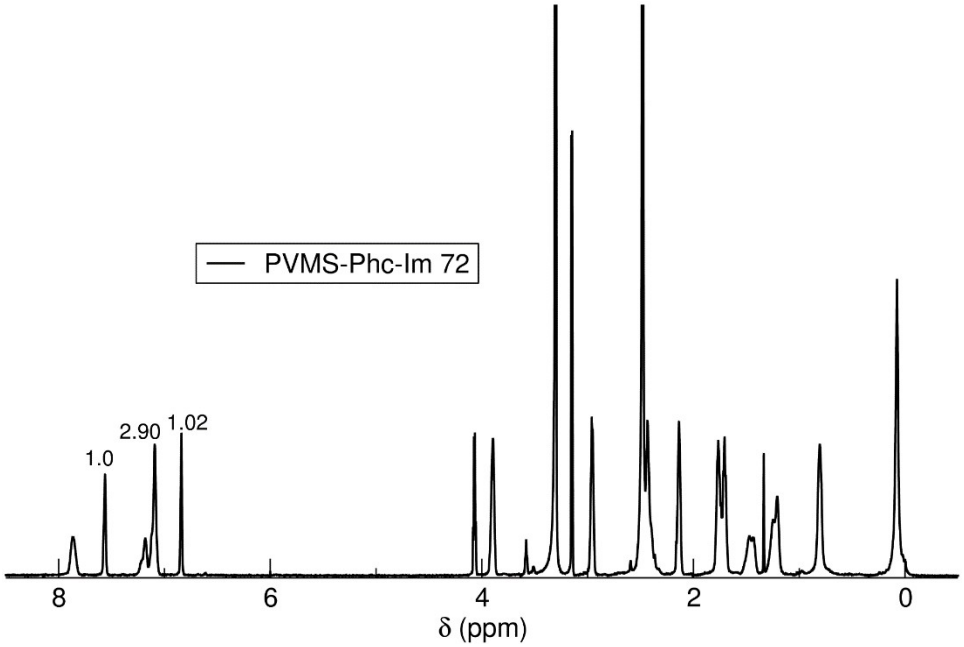

Figure S8. NMR trace for PVMS-Phc-Im with 72% imidazole grafting showing integration ratio between the imidazole and phenyl aromatic peaks. Taken in DMSO-d6.

Polymer SEC:

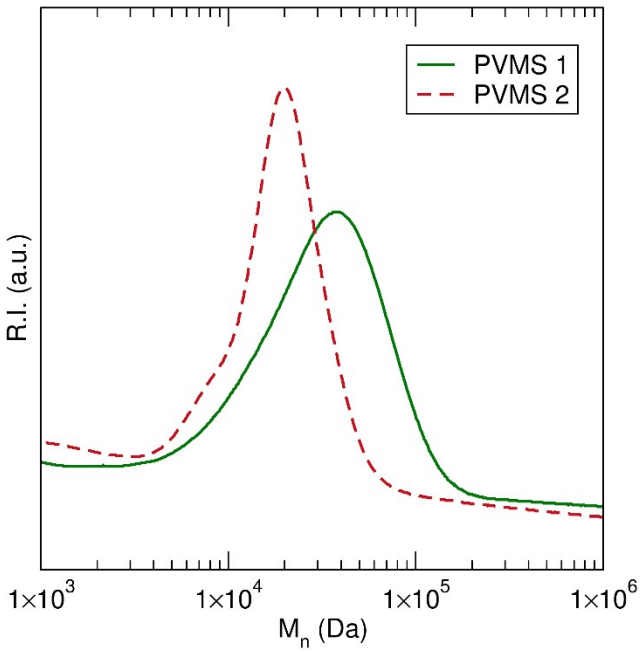

Figure S9. SEC traces for the two batches of PVMS synthesized for this study.

Table S1. SEC results for the backbones synthesized for this study.

Polymer backbone	Used for samples	M_n (kDa)	Đ
PVMS 1	PVMS-Et-Im	29	1.60
PVMS 2	PVMS-Phc-Im	19	1.29

X-ray Scattering

Wide-angle X-ray scattering (WAXS) shows changes in polymer structure with lower grafting density for the ethane-imidazole polymer series but no change for the phenyl-imidazole series (Figure S10). In addition to a broad amorphous halo peak around 0.4 nm, a shoulder peak emerges at about 1 nm as imidazole content within the ethane-imidazole polymers is reduced. This peak is the most intense when no imidazole is present in the polymer, signifying the ethane side chain is responsible for this added structure. The phenyl-imidazole polymers do not show the same feature in X-ray scattering, suggesting that the bulk of the phenyl side chain may be effectively preventing this aggregation. Importantly, the structure determined from X-ray scattering only provides an averaged, static snapshot of these polymers. Since the ion conduction properties are measured at temperatures above the glass transition temperature, these polymers are highly mobile locally, and any aggregation or phase segregation undergoes significant fluctuations with time. These fluctuations likely reduce the importance of this polymer structure on the ion conduction results.

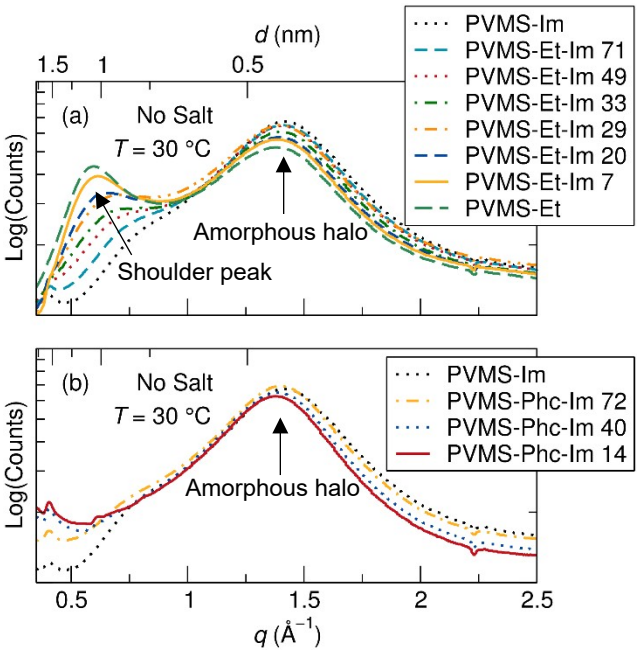

Figure S10. WAXS data for the (a) ethane-imidazole and (b) phenyl-imidazole polymer series *without salt*. The data show additional structure arising in the ethane-imidazole system, with the appearance of a shoulder peak around 0.8 nm to 1.2 nm, which grows in intensity and shifts to larger *d*-spacing as the imidazole content decreases. Interestingly, this shoulder peak is already weakly present in the fully-imidazole-functionalized case, but disappears in the phenyl-imidazole series. It is possible that the feature shifts in location and is obscured by background/detector noise below $q = 0.5$ Å^{-1}.

Salt addition to the polymers often results in the emergence of an ‘ion aggregation’ peak at length scales between 3 nm and 6 nm, as probed via small-angle X-ray scattering (SAXS). The interpretation of this aggregate peak is challenging, but is generally believed to arise from scattering between discrete aggregates, or, for stringy or percolated aggregates, both inter- and intra-aggregate scattering.[1] Thus, for discrete aggregates it measures the spacing between aggregates, while for stringy or percolated aggregates it can also measure the distance between various segments of a single aggregate.

Thermal Characterization

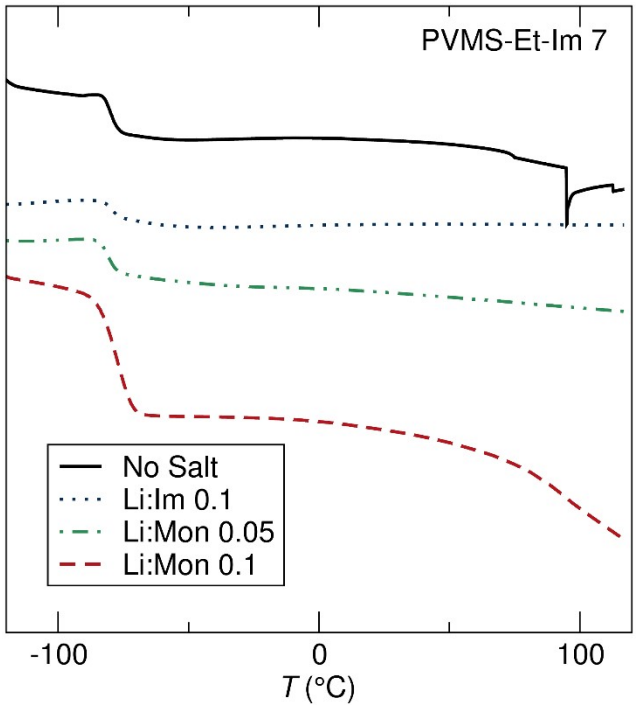

Figure S11. DSC traces indicating T_g for PVMS-Et-Im with 7% imidazole grafting at the various LiTFSI concentrations studied. The sharp peak near 100 °C for the sample without salt is an artifact due to instrument electronic noise.

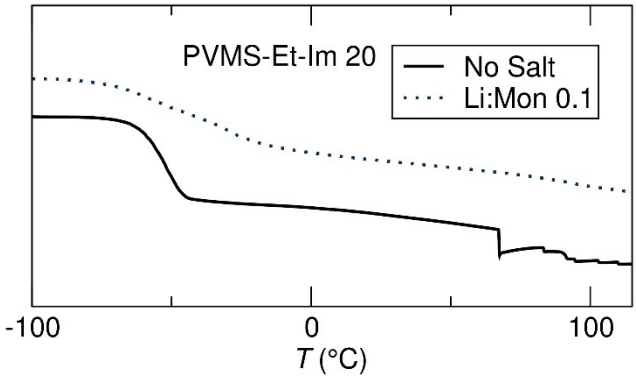

Figure S12. DSC traces indicating T_g for PVMS-Et-Im with 20% imidazole grafting with and without LiTFSI salt. The sharp steps beginning around 60 °C for the sample without salt is an artifact due to instrument electronic noise.

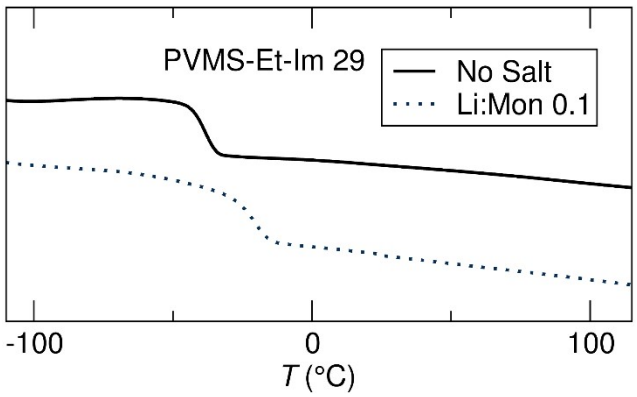

Figure S13. DSC traces indicating T_g for PVMS-Et-Im with 29% imidazole grafting with and without LiTFSI salt.

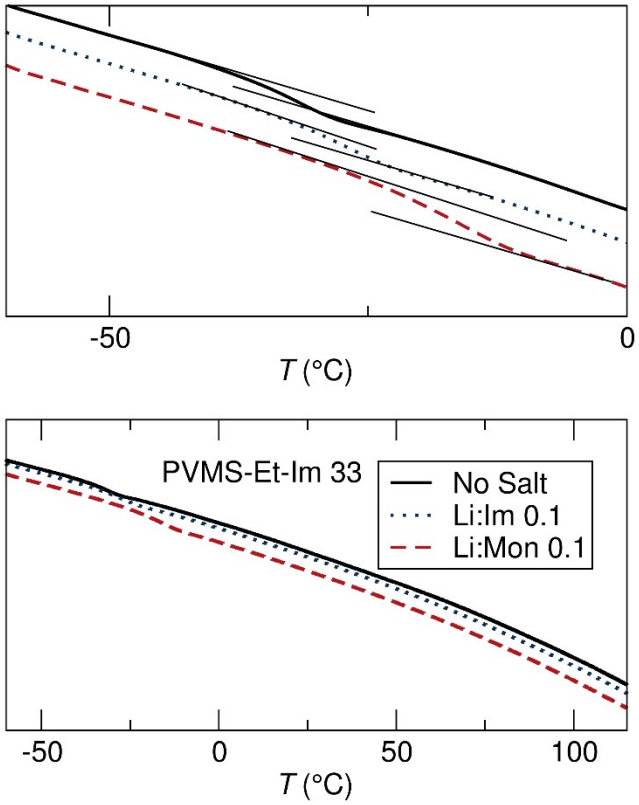

Figure S14. DSC traces indicating T_g for PVMS-Et-Im with 33% imidazole grafting with and without LiTFSI salt. The top plot zooms into the region of interest to show the T_g response for each polymer.

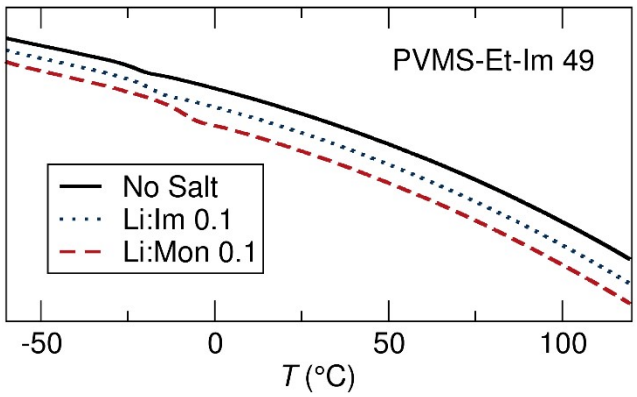

Figure S15. DSC traces indicating T_g for PVMS-Et-Im with 49% imidazole grafting with and without LiTFSI salt.

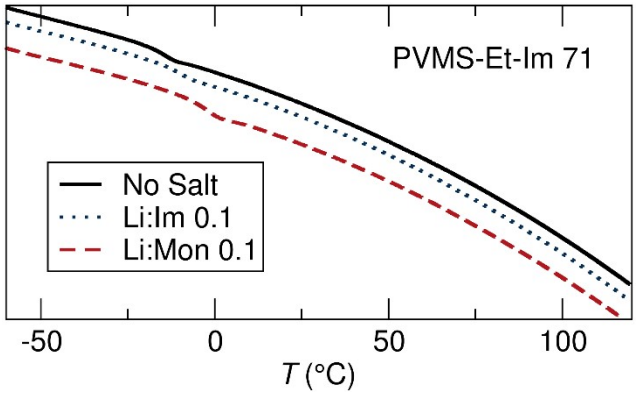

Figure S16. DSC traces indicating T_g for PVMS-Et-Im with 71% imidazole grafting with and without LiTFSI salt.

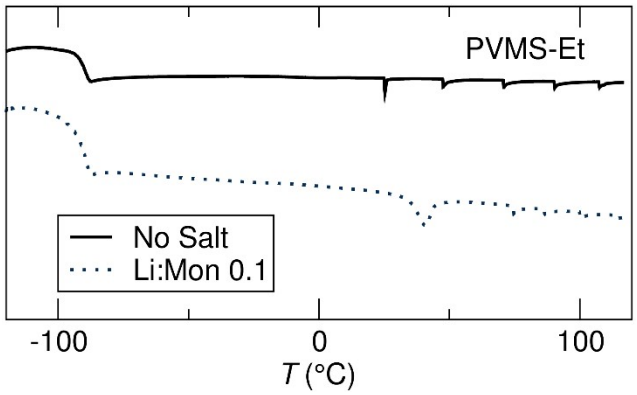

Figure S17. DSC traces indicating T_g for PVMS-Et with and without LiTFSI salt. The sharp peaks above 0°C are electronic noise, while the broader peak at 45 °C for the polymer with salt indicates a melting transition, suggesting a crystalline component due to incomplete salt dissolution.

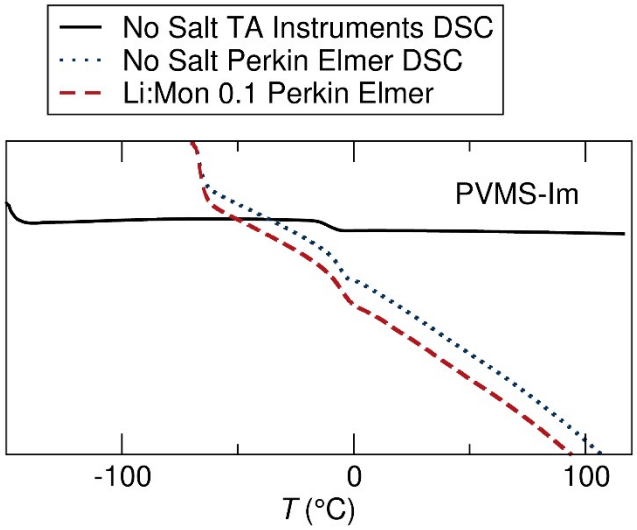

Figure S18. DSC traces indicating T_g for PVMS-Im with and without LiTFSI salt. The polymer without salt was measured on two DSC instruments, with a 5 °C shift in Tg between the two.

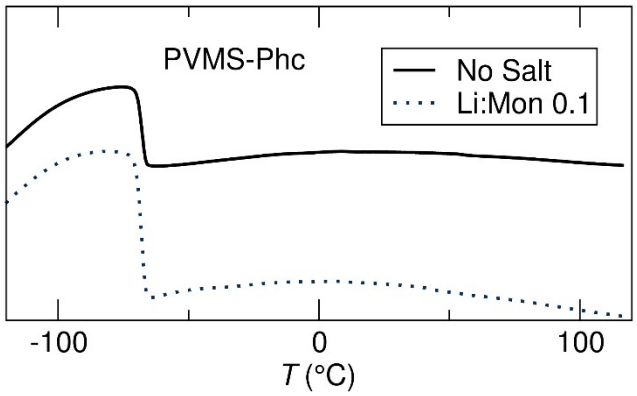

Figure S19. DSC traces indicating T_g for PVMS-Phc with and without LiTFSI salt.

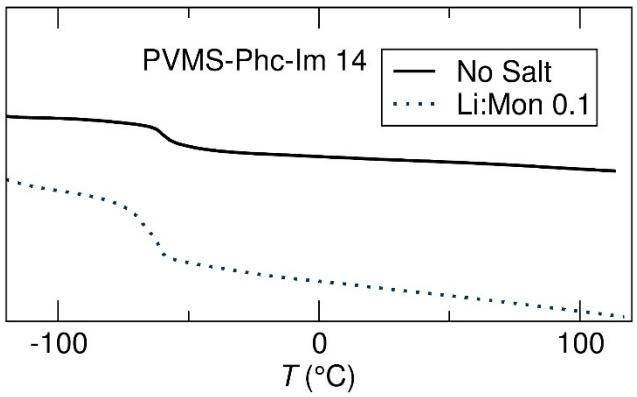

Figure S20. DSC traces indicating T_g for PVMS-Phc-Im with 14% imidazole grafting with and without LiTFSI salt.

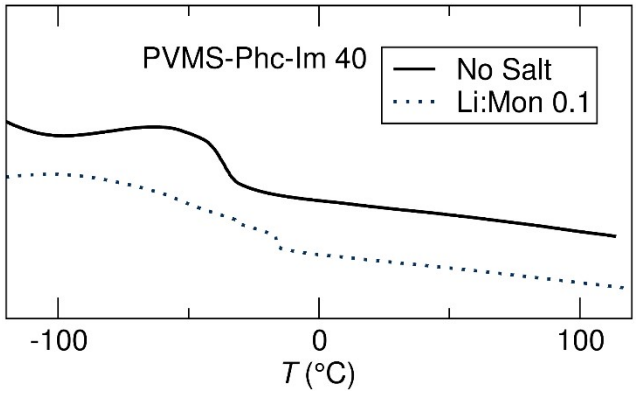

Figure S21. DSC traces indicating T_g for PVMS-Phc-Im with 40% imidazole grafting with and without LiTFSI salt. The Tg for the polymer with salt is too broad to accurately determine, but looks to be within the same range as the polymer without salt – this value was used in the T_g normalization for conductivity.

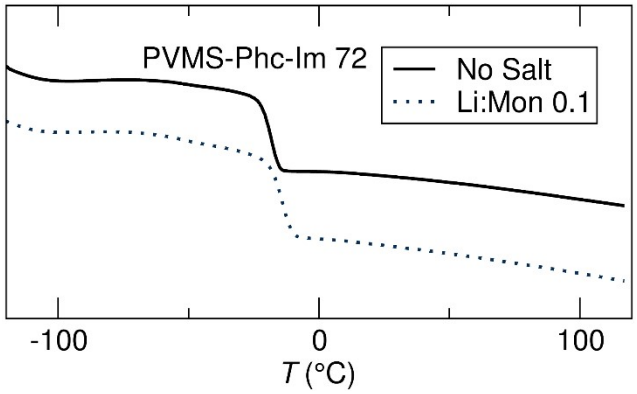

Figure S22. DSC traces indicating T_g for PVMS-Phc-Im with 72% imidazole grafting with and without LiTFSI salt.

T_g trend with grafting density

The T_g behavior of random copolymers and polymer blends can sometimes be described by the Fox Equation, which assumes heat capacities of the polymers are invariant with temperature, and the change in heat capacities and T_gs of the two components do not differ greatly

$$\frac{1}{T_g} = \frac{w_1}{T_{g,1}} + \frac{w_2}{T_{g,2}}$$

As can be seen in Figure S23 and S24, this relationship does not hold well for either of the two copolymer series explored in this study. This is likely due to the hydrogen bonding capability of

the amide functional group within the imidazole sidechain, as well as significant dielectric contrast between the two copolymers.

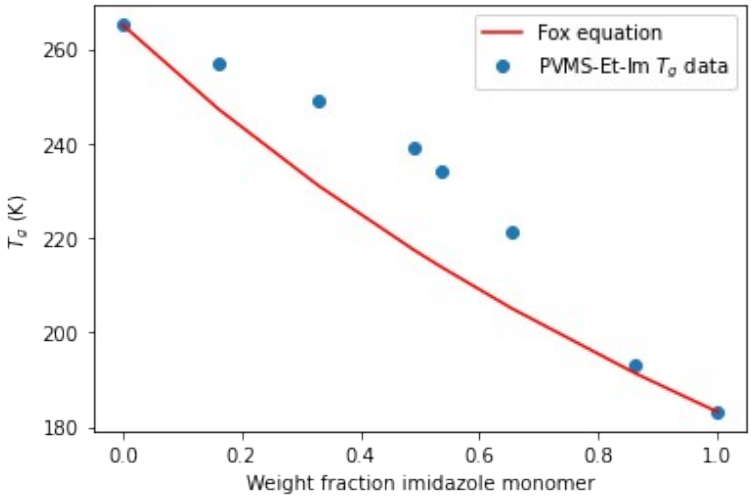

Figure S23. T_g versus imidazole weight fraction for the PVMS-Et-Im polymer series without salt addition.

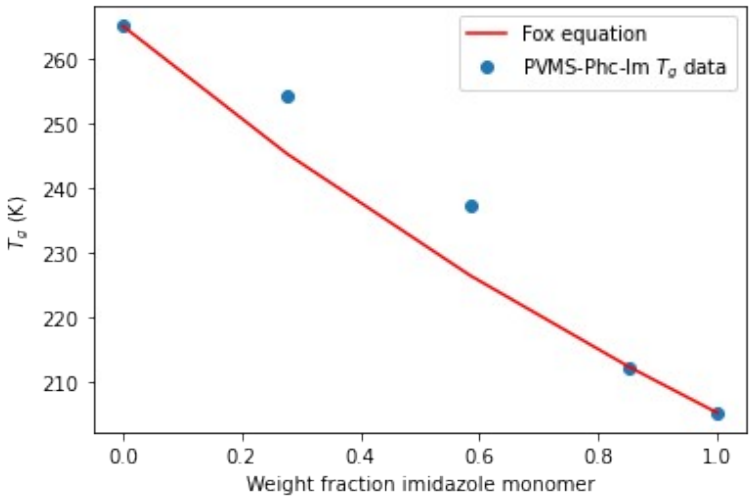

Figure S24. T_g versus imidazole weight fraction for the PVMS-Phc-Im polymer series without salt addition.

Ionic Conductivity

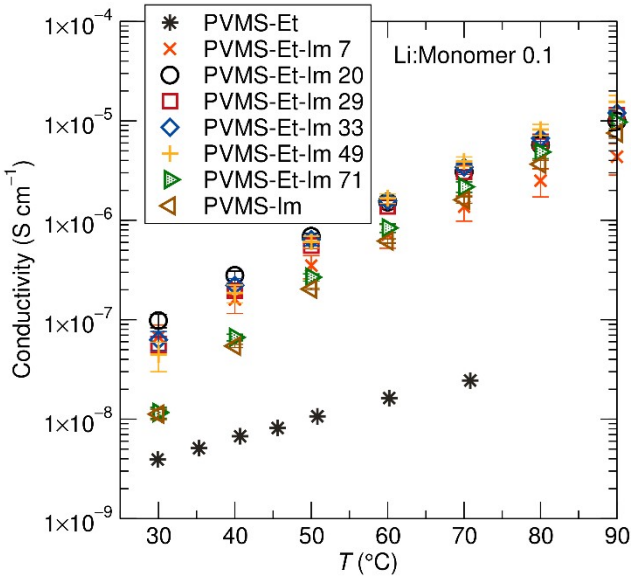

Figure S25. Total ionic conductivity as a function of temperature for the PVMS-Et-Im series at a salt concentration of Li:Monomer of 0.1. Error bars are shown as the standard deviation from the mean (for three samples) for all polymers except PVMS-Et, for which only one sample was measured.

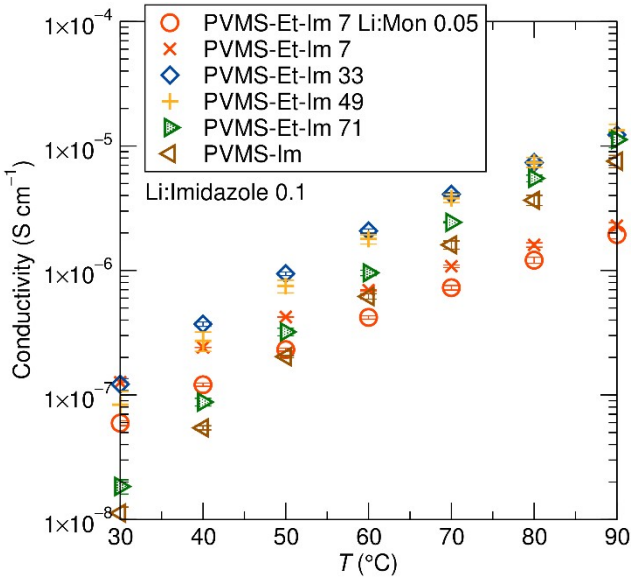

Figure S26. Total ionic conductivity as a function of temperature for the PVMS-Et-Im series at a salt concentration of Li:Imidazole of 0.1. Error bars are shown as the standard deviation from the

mean (for three samples) for all polymers except PVMS-Et-Im 7 Li:Imidazole = 0.1, for which two samples were measured. PVMS-Et-Im 7 Li:Monomer = 0.05 is also included.

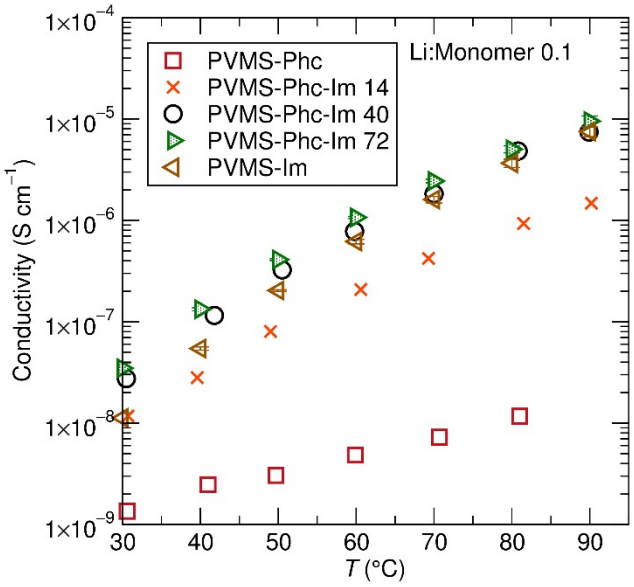

Figure S27. Total ionic conductivity as a function of temperature for the PVMS-Phc-Im series at a salt concentration of Li:Monomer of 0.1. Three samples are averaged for PVMS-Phc-Im 72 and PVMS-Im while only one sample was measured for the other grafting densities.

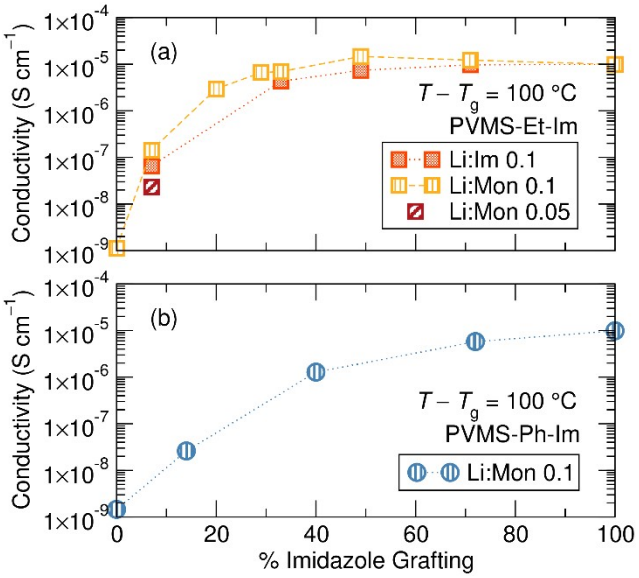

Figure S28. Ionic conductivity at T–T_g = 100 for the (a) ethane-imidazole and (b) phenyl-imidazole grafting series. T_g-normalized conductivity shows an expected increase with increasing salt concentration from Li:Im 0.1 to Li:Mon 0.1.

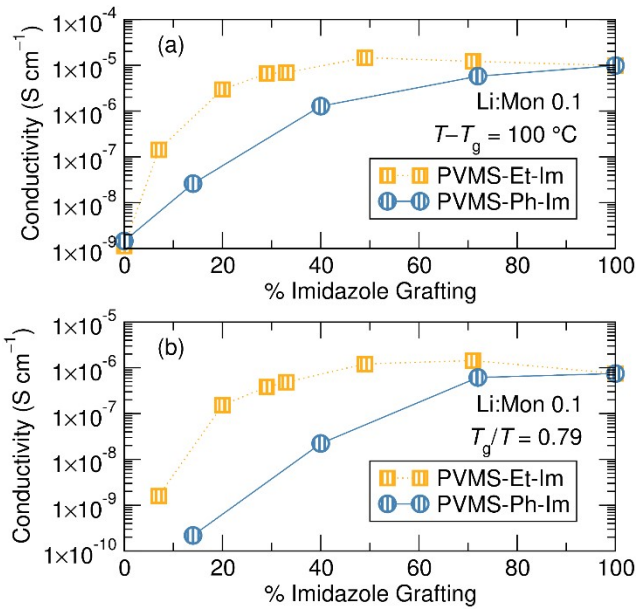

Figure S29. (a) Total ionic conductivity for both grafting series at a T_g-normalized temperature of $T - T_g = 100$ °C as shown in Figure 5. (b) Total ionic conductivity for both grafting series at a T_g-normalized temperature of $T_g/T = 0.79$, resulting in very similar behavior as seen in (a).

Table S2. Temperature and conductivity values for samples at $T - T_g = 100$ at a salt concentration of Li:Monomer = 0.1

Sample	$T = 100 + T_g$ (°C)	Conductivity (S/cm)	Standard deviation
V-Et Li:Mon 0 .1	11	1.13×10^{-9}	N/A
VEI-7 Li:Mon 0 .1	35	1.05×10^{-7}	3.04×10^{-8}
VEI-20 Li:Mon 0 .1	69	2.88×10^{-6}	7.5×10^{-8}
VEI-29 Li:Mon 0 .1	80	6.16×10^{-6}	4.08×10^{-7}
VEI-33 Li:Mon 0 .1	81	7.11×10^{-6}	5.13×10^{-7}
VEI-49 Li:Mon 0 .1	89	1.47×10^{-5}	2.21×10^{-6}
VEI-71 Li:Mon 0 .1	96	1.41×10^{-5}	2.49×10^{-6}
V-Im Li:Mon 0.1	93	9.21×10^{-6}	1.09×10^{-6}
V-Ph Li:Mon 0.1	32	1.45×10^{-9}	N/A
VPcI 14 Li:Mon 0.1	38	2.60×10^{-8}	N/A
VPcI 40 Li:Mon 0.1	64	1.28×10^{-6}	N/A
VPcI 72 Li:Mon 0.1	87	7.93×10^{-6}	8.84×10^{-7}

Normalizing by salt concentration and imidazole content

The imidazole grafting density can be converted to a molar density by dividing the grafting percentage by the molar mass of the polymer. This is shown in Figure S30.

$$\frac{mmol\ imidazole}{g\ polymer} = \frac{\%\ imidazole\ grafting}{100} \frac{1}{polymer\ mass\left(\frac{g}{mol}\right)} * 1000$$

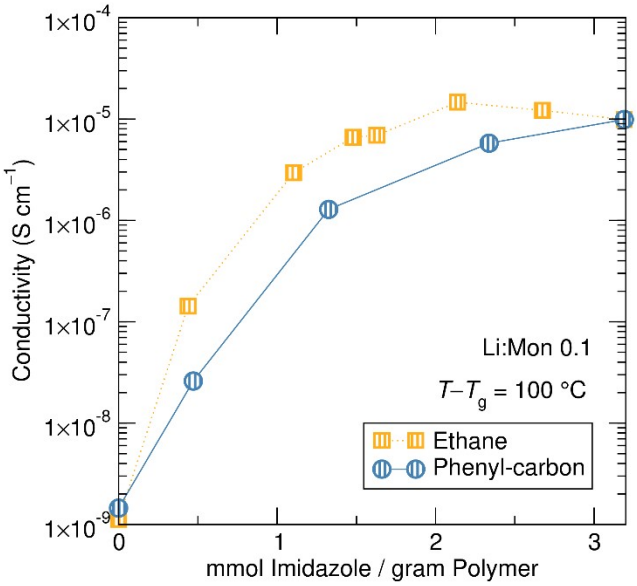

Figure S30. Ionic conductivity at T-T_g = 100 versus molar imidazole content per gram polymer.

To generate Figure 5b, the molar conductivity was calculated by dividing the ionic conductivity by the molar salt concentration. The molar salt concentration is estimated with a polymer density of 1 g/cm^3 (and also assuming polymer density does not change appreciably with salt addition and grafting density), using the following equation:

$$salt\ concentration\left(\frac{mol}{cm^3}\right)$$
$$= polymer\ density\left(\frac{g}{cm^3}\right)\frac{1}{polymer\ mass\left(\frac{g}{mol}\right)}Li{:}Mon\ salt\ concentration$$
$$\left(\frac{mol\ salt}{mol\ polymer}\right)$$
$$= \frac{1}{polymer\ mass\left(\frac{g}{mol}\right)}Li{:}Mon\ salt\ concentration\left(\frac{mol\ salt}{mol\ polymer}\right)$$

Values for the salt concentrations are given in Table 1 in the main text. The molar ionic conductivity divides the ionic conductivity by that salt concentration. While assuming constant polymer density is certainly not strictly correct, it is also not likely to change by more than a factor of 1.5, which would not significantly change the observed results.

Solid-state NMR:

Diffusion Coefficient Fitting curves

Diffusion coefficients in this study were measured using pulsed-field gradient NMR (PFG-NMR). The diffusion NMR pulse sequence is made up of four steps, the excitation, application of spatial encoding, evolution to allow diffusion of the relevant ions and the subsequent removal of the spatial encoding. The diffusion experiment involves varying the gradient strength and monitoring the change in signal intensity. The sequence used in these measurements includes a stimulated echo rather than a hard 180° pulse in the evolution stage. This serves to protect the NMR signal from T_2 decay while the ions are allowed to diffuse. Figure S31 shows a schematic of the pulse sequence used in this study. It is also possible to split the gradient pulses in two halves, separated by a 180° hard RF pulse, which is termed a bipolar pulse. The bipolar pulses act to eliminate any background magnetic field gradients; however, it was observed in this study that the signal to noise obtained from the sequence was around half that of the sequence shown in Figure S31. Therefore, in this study the bipolar pulses were not used, as the signal in these measurements were prohibitively small. Values were compared between sequences with and without the bipolar pulses and were seen to be the same within error.

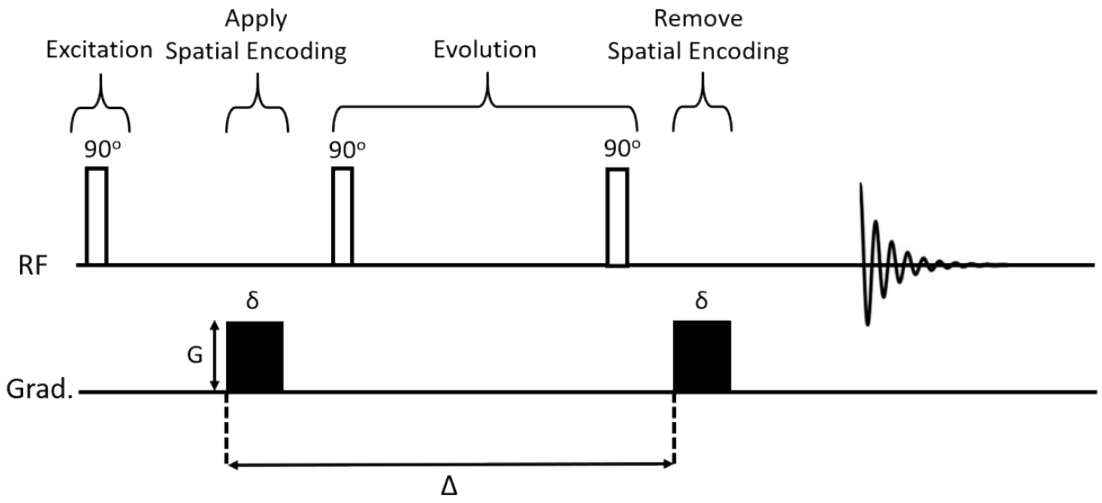

Figure S31: PFG-NMR diffusion stimulated echo pulse sequence.

In the diffusion experiment, the gradient strength is varied and the intensity is monitored. The stronger the gradient strength applied the greater the signal attenuation that will occur. The signal attenuation ($S(G)$) as a function of gradient strength (G) can be described in terms of the self-diffusion coefficient (D), gyromagnetic ratio (γ), diffusion time (Δ), gradient pulse duration (δ) and a pre-exponential factor (S_0), as shown in equation S1.

$$S(G) = S_0 exp\left(- D\gamma^2 G^2 \delta^2 \left(\Delta - \frac{\delta}{3} \right) \right) \quad (S1)$$

The gradient values are selected based on the diffusion of the sample at a given temperature. Therefore, for each measurement the set of gradient values were determined by doing calibration step.

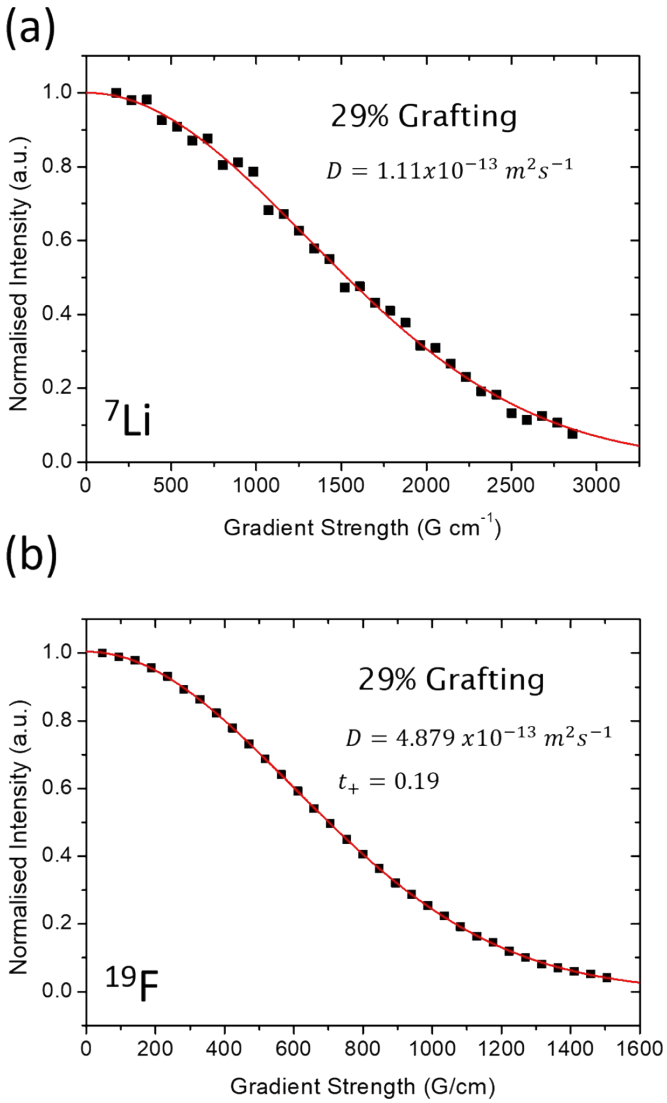

Figure S32: PFG-NMR diffusion decay curve for the PVMS-Et-Im 29 polymer electrolyte sample with 0.1 Li:Monomer LiTFSI salt, measured at 81.4 °C (354.6 K) for the (a) Li^+ (^{7}Li) and (b) $TFSI^-$ (^{19}F) ions.

Figure S32 shows an example PFG-NMR diffusion decay curve for the 29% imidazole grafting density polymer measured at 81.4 °C (354.6 K) for both the Li^+ (^{7}Li, Figure S32a) and TFSI (^{19}F, Figure S32b) ions. For this particular sample, the diffusion constants obtained from these curves are $1.11x10^{-13}$ m^2s^{-1} and $4.88x10^{-13}$ m^2 s^{-1} for the Li^+ and $TFSI^-$ ions, respectively. Therefore, the cation transference number t_+ for this system at 81.4 °C is 0.19, calculated as follows:

$$t_+ = \frac{\sigma_+}{\sigma_+ + \sigma_-} = \frac{D_{Li+}}{D_{Li+} + D_{TFSI-}} \quad \text{(S2)}$$

The magnitude of the activation energies for the diffusion and conductivity are similar, which is expected in the absence of correlated diffusion. Interestingly, the 100 % grafted sample exhibits

the fastest diffusion for both the Li^+ and $TFSI^-$ ions, followed by the 29 % grafted sample, with the slowest diffusing sample being the 71 % grafted polymer electrolyte. Activation energies for ionic diffusion can be estimated by fitting an Arrhenius equation to PFG-NMR data. These activation energies are determined to be 68.4 kJ mol^{-1}, 90.2 kJ mol^{-1} and 72.5 kJ mol^{-1} for Li^+ ions in the 29 %, 71 % and 100 % grafted samples, respectively. For $TFSI^-$ ions, activation energies of 61.8 kJ mol^{-1}, 73.5 kJ mol^{-1} and 73.6 kJ mol^{-1} are obtained for the 29 %, 71 % and 100 % grafted samples, respectively. The limited temperature range probed may result in inaccurate diffusion barriers; however, these activation energies are still used as a rough estimate to compare these diffusion measurements to alternate NMR techniques. It should be noted that the conductivity and diffusion measurements are expected to follow Vogel-Fulcher-Tamman (VFT) theory rather than Arrhenius behavior, however, over the limited temperature range measured the latter theory provides good estimates. For comparison, the activation energies determined from the total ionic conductivity measurements are 69.2 kJ mol^{-1}, 77.8 kJ mol^{-1} and 98.3 kJ mol^{-1} for the 29 %, 71 % and 100 % grafted samples respectively.

Calculating expected ionic conductivity

The NMR-derived conductivity is calculated using the Nernst-Einstein equation:

$$\sigma = \frac{N_a e^2 C}{k_B T}(D_+ + D_-) \quad \text{(S3)}$$

where N_a is Avogadro's number, e is the charge on an electron, C is the concentration of ions in the system, k_B is Boltzmann's constant and T is the temperature of the measurement, in Kelvin. The ion concentration has been estimated assuming a polymer density of 1 g cm^{-3} and complete salt dissociation. The calculated conductivities from each ion (σ_+ and σ_-) as well as the total calculated conductivity are also presented in Table 2.

The ratio of the EIS measured to NMR-derived conductivity, for each sample, provides an estimate of the percentage of conducting ions, where 100 % represents full salt dissociation. These values are 64.5 %, 91.9 % and 45.5 % for the 29 %, 71 % and 100 % imidazole grafted samples at 72.7 °C.

Line width Analysis

The NMR line width is inversely proportional to the spin-spin relaxation time (T_2), which in turn depends on the mobility of the species under investigation. As ion dynamics become slower, for instance at lower temperatures, the T_2 value decreases and tends to zero, while the NMR signal becomes broader.

such measurements. The activation energies are significantly smaller than the corresponding energies obtained for the diffusion process. T_1 experiments probe typically ns timescale dynamics, which are orders of magnitude shorter than that of diffusion, and instead probe very local

dynamics, such as reorientation and reptation. It is for this reason that the activation energy obtained is much smaller than the activation energy obtained from that of the diffusion process.

$T_{1\rho}$ Analysis

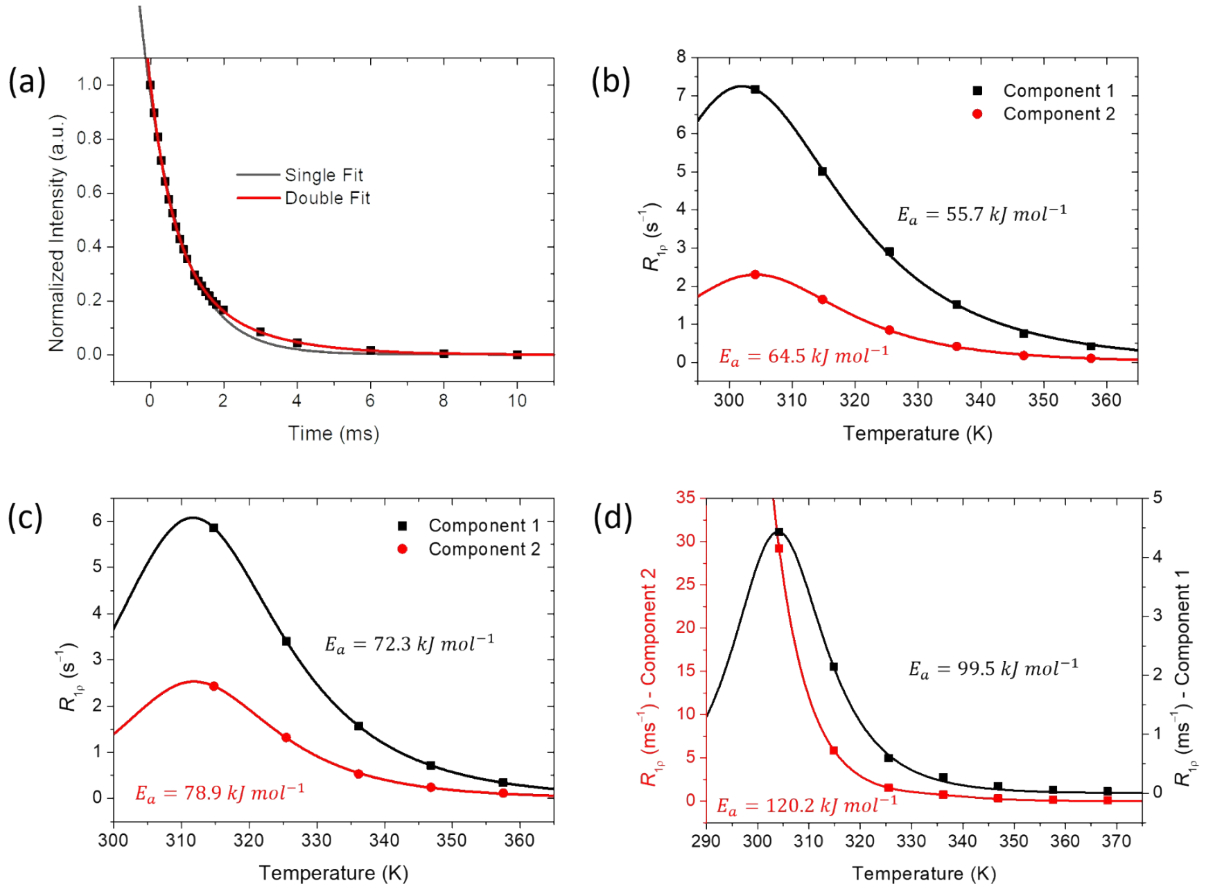

Figure S33. (a) ^{7}Li example $T_{1\rho}$ decay curve for the 71 % imidazole grafted polymer sample with ethane side chains with 0.1 Li:monomer LiTFSI added, measured at 63 °C, with 10 kHz spin-locking frequency. Two components found for all samples and shown as a function of temperature for the (b) 29 % grafted sample, (c) 71 % grafted and (d) 100 % grafted polymer electrolytes.

Figure S33a shows an example $T_{1\rho}$ decay curve for the 71 % imidazole grafted sample measured at 63 °C using a spin-locking frequency of 10 kHz. The $T_{1\rho}$ intensity (S) decay curves as a function of time (t) are fitted to an exponential decay function in the form of Equation S4 for a single exponential fit and Equation S5 for a biexponential (two component) fit. It can be clearly observed from Figure S33a that a second component is needed to fit the data well.

$$S = S_0 e^{-t/T_{1\rho}} \quad \text{(S4)}$$

$$S = S_1 e^{-t/T_{1\rho,1}} + S_2 e^{-t/T_{1\rho,2}} \quad \text{(S5)}$$

where S_1 and S_2 are pre-exponential terms that denote the fractional occupation of each component. Interestingly, the values of S_1 and S_2 do not seem to be dependent on temperature.

The more prevalent lithium environment (component 1) is also more mobile, as revealed by the lower activation energy obtained from fits to the temperature-dependent relaxation rate $R_{1\rho,DD}$ (Figure S33b,c). The data were fitted to the theoretical equation for the dipole-dipole relaxation ($R_{1\rho,DD} = \frac{1}{T_{1\rho,DD}}$), which depends on the spin-lock frequency (ω_1), the Larmor frequency (ω_0), an arbitrary constant (k) and the rotational correlation time (τ_c), and is expressed in Equation S6.

$$R_{1\rho,DD} = \frac{1}{T_{1\rho,DD}} = k\left(\frac{3\tau_c}{1+4\omega_1^2\tau_c^2} + \frac{5\tau_c}{1+\omega_0^2\tau_c^2} + \frac{2\tau_c}{1+4\omega_0^2\tau_c^2}\right) \quad \text{(S6)}$$

In order to relate equation S6 to the temperature study in Figure S33 the correlation time is assumed Arrhenius in nature (see equation S3 above). The fit shown in Figure S33b for the 29 % grafting density polymer allows activation energies to be determined for the two components, namely 55.7 kJ mol^{-1} and 64.5 kJ mol^{-1} for component 1 and 2, respectively. Therefore, component 1 is the faster diffusing environment and is also the dominant component. The 71 % grafted sample, displayed in Figure S33c, exhibits very similar trends with component 1 as the faster, and dominant environment. However, both components are less mobile for the 71 % grafted polymer sample as the activation energies of component 1 and 2 are 72.3 kJ mol^{-1} and 78.9 kJ mol^{-1}, respectively. The activation energies increase further for the 100 % grafted polymer sample (Figure S33d) up to 99.5 kJ mol^{-1} and 120.2 kJ mol^{-1} for the two components.

Chemical shift analysis

If two chemically distinct site are in exchange with one another, then it is possible to probe exchange dynamics by simply monitoring the evolution of the chemical shift with temperature. In the fast exchange regime, the observed chemical shift is a weighted average of the two environments and will be temperature dependent if the population of the two sites changes with temperature. Figure S34a shows the evolution of the Li^+ chemical shift with temperature. All ^{7}Li spectra were fitted with two peaks, one broad component and a narrower component, but the values displayed in Figure S34 are for the narrow peak as the broader component was difficult to fit with certainty (example shown in Figure S35).

The curve in Figure S34a for the 29 % imidazole grafted sample is characteristic of exchange. The observed chemical shift of an exchanging peak is a weighted average of the two environments. For an exchanging peak, the chemical shift can be described by the following equation:

$$\delta = \frac{exp\left(\frac{T\Delta S - \Delta H}{RT}\right)\delta_A + \delta_B}{1 + exp\left(\frac{T\Delta S - \Delta H}{RT}\right)} \quad (S7)$$

where δ_A and δ_B are the chemical shift of the two exchanging peaks, ΔS is the change in entropy, ΔH is the change in enthalpy, R is the gas constant and T is the absolute temperature of the sample. This equation describes exchange on the sub-millisecond exchange timescale. This equation was used to fit the data for the 29 % grafted sample in Figure S34a. The higher grafting density samples do not show the same behavior over the temperature range considered here, which could either indicate that there is no exchange between the different sites, the chemical shift of the two pure peaks of the exchanging sites are close together, or the exchange is happening on a different timescale than the NMR measurement.

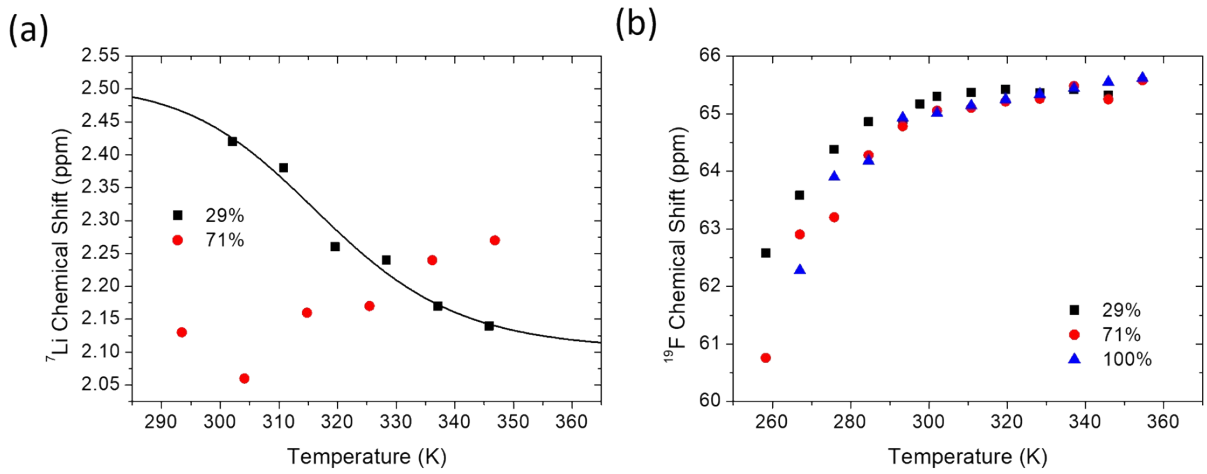

Figure S34: (a) ^{7}Li NMR and (b) ^{19}F NMR chemical shift as a function of temperature. All samples consist in a 0.1 Li:monomer ratio of LiTFSI added to the polymer.

Interestingly, the corresponding chemical shift data for the ^{19}F measurements shown in Figure S36b exhibit insignificant changes at room temperature and above, however, below ambient temperature the chemical shift for all samples change rapidly with temperature. We note that a chemical shift difference of this magnitude is unlikely to be caused by a simple slow-down of dynamics.

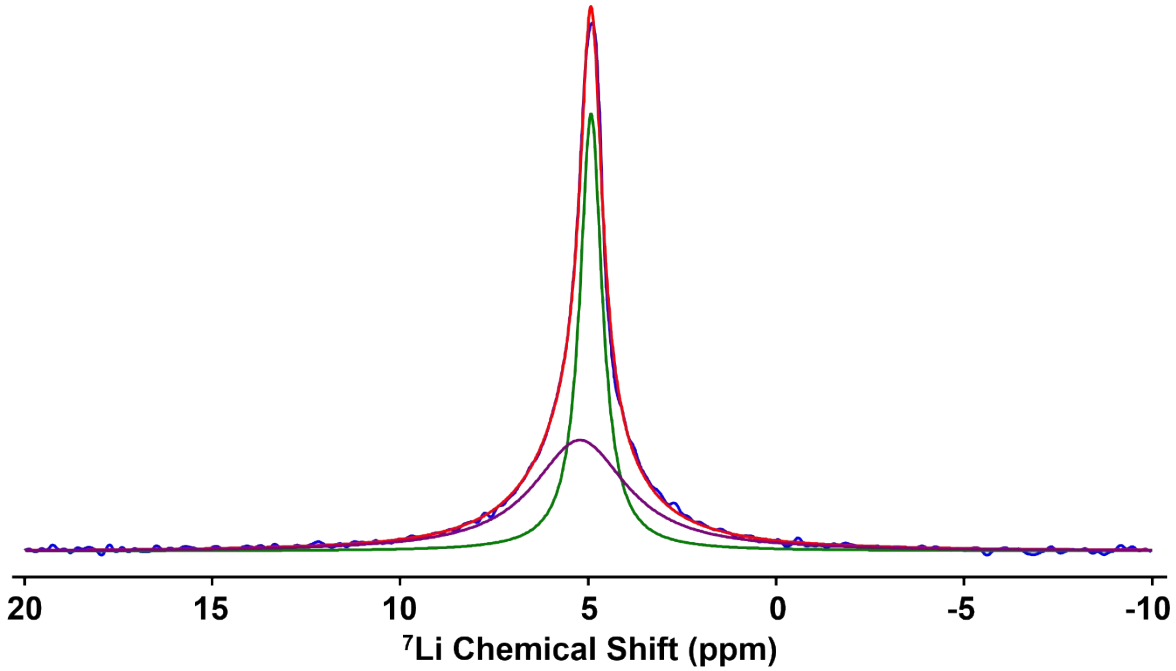

Figure S35: ^{7}Li NMR spectrum of the 71 % imidazole grafting density polymer with 0.1 Li:monomer LiTFSI salt concentration at 72.7 °C. The data (blue line) has been fitted with two components (green and purple lines) and also shows the overall fit (red line).

References

(1) Buitrago, C. F.; Bolintineanu, D. S.; Seitz, M. E.; Opper, K. L.; Wagener, K. B.; Stevens, M. J.; Frischknecht, A. L.; Winey, K. I. Direct Comparisons of X-ray Scattering and Atomistic Molecular Dynamics Simulations for Precise Acid Copolymers and Ionomers. *Macromolecules* **2015**, *48*, 1210–1220.

(2) Schauser, N. S.; Grzetic, D. J.; Tabassum, T.; Kliegle, G. A.; Le, M. L.; Susca, E. M.; Antoine, S.; Keller, T. J.; Delaney, K. T.; Han, S.; Seshadri, R.; Fredrickson, G. H.; Segalman, R. A. The Role of Backbone Polarity on Aggregation and Conduction of Ions in Polymer Electrolytes. *J. Am. Chem. Soc* **2020**, *142*, 7055–7065.

(3) Schauser, N. S.; Sanoja, G. E.; Bartels, J. M.; Jain, S. K.; Hu, J. G.; Han, S.; Walker, L. M.; Helgeson, M. E.; Seshadri, R.; Segalman, R. A. Decoupling Bulk Mechanics and Mono- and Multivalent Ion Transport in Polymers Based on Metal-Ligand Coordination. *Chem. Mater*. **2018**, *30*, 5759–5769.